Isotropic−Nematic Phase Transition of Dispersions of Multiwall Carbon Nanotubes

Wenhui Song† and Alan H. Windle*

Department of Materials Science and Metallurgy, University of Cambridge, Pembroke Street, Cambridge, CB2 3QZ, U.K.

Received November 10, 2004; Revised Manuscript Received March 17, 2005

ABSTRACT: The unequivocal identification of lyotropic phases in carbon nanotube suspensions has recently been announced (*Science* **2003**, *302*, 1363). Here one aspect of that study is explored in further detail. The isotropic−nematic phase transition has been observed in an aqueous dispersion of multiwall carbon nanotubes (MWNTs) using reflected polarized light microscopy. The coexistence of the two phases over a significantly wide range of concentration is attributed to the polydispersity of nanotube dimensions and straightness, the longer and thicker nanotubes packing preferentially in the anisotropic phase. Above a critical concentration, a Schlieren texture characteristic of the nematic phase is apparent in the dispersion. A sufficiently thin film of a nematic dispersion is transparent enough to enable examination in transmitted polarized light. The characteristic features of the optical texture are related to the corresponding direct FEGSEM images of the nanotubes in dried samples.

Introduction

Carbon nanotubes (CNTs), with their unique electronic and mechanical properties,[2] are promising components for a broad range of applications from molecular electronics to strong, lightweight composites. However, processing of nanotubes still remains a significant challenge if their full potential is to be realized. Efforts have been made within the past decade to achieve nanotube alignment during growth by chemical vapor deposition (CVD)[3−5] and by postsynthesis fabrication strategies,[6−18] which are of particular interest as mass production methods become available. Such strategies include the cutting of a nanotube−polymer composite,[7] wet- or dry-spinning,[4,5,8,9] surface-rubbing and surface assembly,[11−13] electric or magnetic field orientation,[14−16] polymer wrapping,[17] and liquid crystal routes.[18] It has also been reported that composite fiber spun from a dispersion of poly(vinyl alcohol) and surfactant containing 60% SWNTs are tougher than any natural or synthetic organic fibers.[10] A significantly increased storage modulus (40 GPa) for SWNT/epoxy composites has also been achieved by aligning nanotubes under a high magnetic field (13.7 T)[16] which is in line with predictions.[19] While this latest progress has proved that the alignment of nanotubes plays a significant role in high performance nanotube composites, the development of practical alignment-control processing methods still remains a challenge.

Processing of carbon nanotubes from a carbonaceous mesophase precursor (a discotic liquid crystal) is well established as a route to quality graphite materials.[20] Carbon nanotubes can be considered as a type of highly conjugated, rigid-rod macromolecules, and interesting parallels drawn with "rigid rod" macromolecular systems, such as that used to make Kevlar fiber. The recent announcement of the liquid crystalline phase of both MWNT aqueous dispersions[1] and SWNT in superacid dispersions[21] point to a novel route to large-scale alignment of the nanotubes during the processing. The lyotropic aqueous system of MWNTs serves as a model for further study of liquid crystalline behavior of nanoparticles, with the added advantage of the availability of a range of MWNTs with different diameters and lengths arising from improved control of synthesis and acid treatment.[22] The fact that the nanotubes are much more electron beam resistant than other nanoscale rigid rod systems, such as DNA[23] and tobacco mosaic virus (TMV),[24,25]opens up new opportunities to examine the self-organizing behavior of liquid crystalline systems at a resolution sufficient to identify the individual nanotubes.

Orientation-dependent repulsion forces between the rod-shape molecules or particles are principally responsible for the stabilization of lyotropic liquid crystalline systems. However, carbon nanotubes, as synthesized, are strongly hydrophobic and generally have very low solubilities in all solvents. While various methods, such as oxidation,[26] grafting, wrapping, and surfactant addition,[6] have been developed for dispersing and solubilizing CNTs, the production of uniform and ordered assemblies remains a challenge. Previous studies suggest that a dilute carbon nanotube suspension is analogous to a polymeric solution, with an abrupt increase in gradient of the viscosity−concentration profile as the gel point is approached at a concentration of ∼0.5 vol %.[27]

Here we report the details of phase transition from the isotropic phase to the lyotropic nematic phase in the aqueous dispersion of carefully characterized MWNTs.

Experimental Methods

The starting materials are multiwall carbon nanotubes synthesized in our laboratory by pyrolysis of a solution of ferrocene in toluene.[22] The injection CVD method in this configuration gives good control of nanotube dimensions through adjustment of ferrocene concentration, gas flow rate, and injection time. The nanotubes produced are unentangled and fairly straight with an outer diameter in a range of 10−120 nm, an inner diameter of about 5−10 nm and a length range from 20 μm to several hundres micrometers. The product

* Corresponding author. E-mail: ahw1@cam.ac.uk.
† Present address: Wolfson Centre for Materials Processing, Brunel University, Uxbridge, West London, UB8 3PH, U.K. E-mail: wenhui.song@brunel.ac.uk.

10.1021/ma047691u CCC: $30.25
Published on Web 06/16/2005

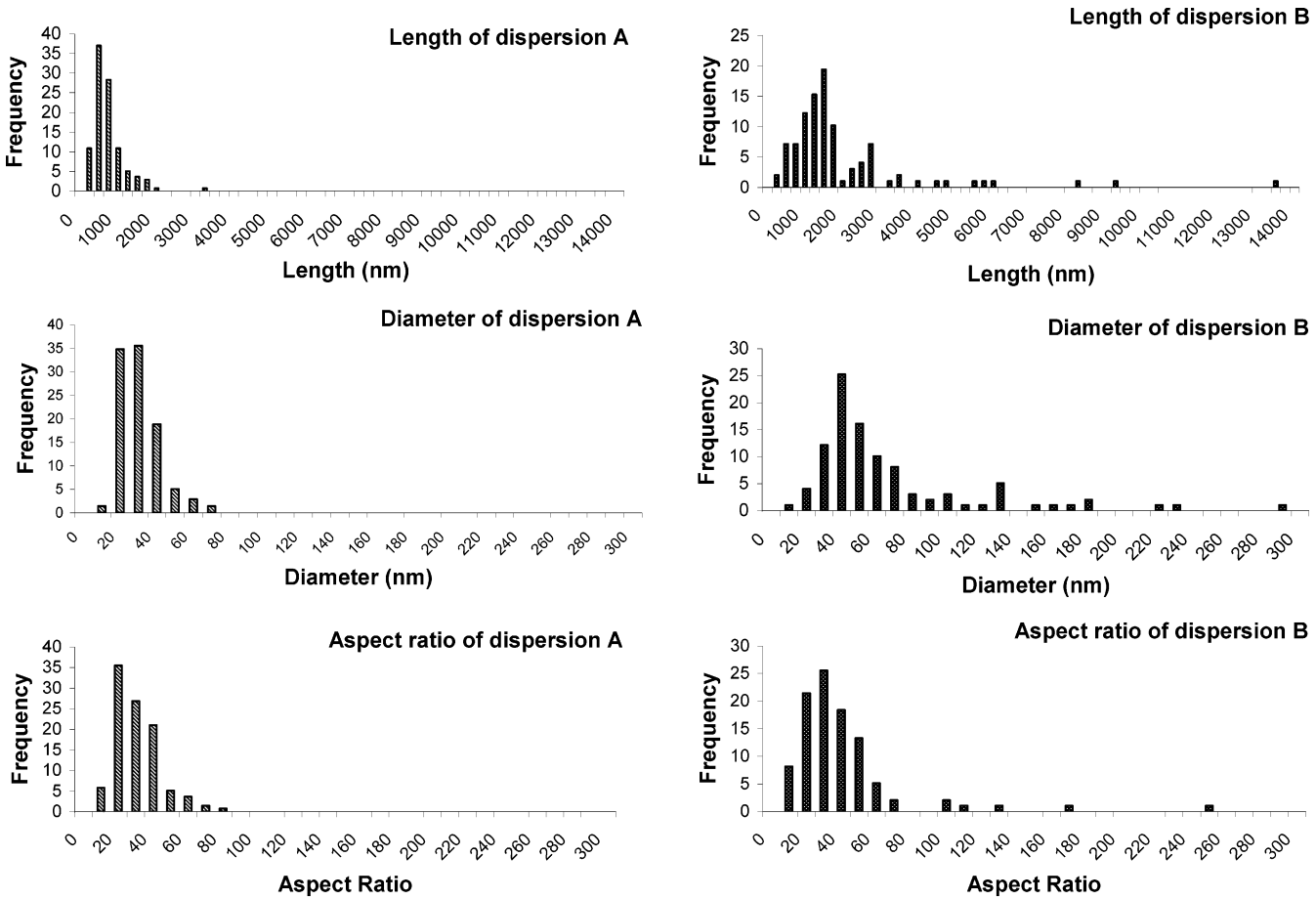

Figure 1. Diameter, length and aspect ratio distribution plots of oxidized multiwall carbon nanotubes of dispersions A and B.

was characterized using a JEOL 6340F field emission gun scanning electron microscope (FEGSEM) and a Renishaw 1000 micro-Raman spectrometer with using a 514 nm excitation laser.

The method of acid treatment described in[28,29] was used to oxidize the multiwall carbon nanotubes to ensure compatibility with water as the suspending medium. The nanotubes (1 g) were suspended in a mixture (250 mL) of concentrated sulfuric acid and nitric acid (3:1 volume ratio) and sonicated in a water bath at 50 °C for 24 h (dispersion A) or 12 h (dispersion B). The resultant suspension was then diluted with 400 mL of deionized water and filtered with water over a 400 nm pore membrane (PTFE) until the water passing through the filter had a pH of between 6 and 7. The dispersions were stable over long periods (>1 year) and could be filtered or diluted to the desired concentration. They had a pH of 3−3.5 at 24 °C.

The weight concentration of the dispersion was determined by pipetting a known volume (V) of the dispersion, followed by weighing before and after drying, the volume fractions being calculated on the basis of a multiwall nanotube density of 1.8 g/cm^3. The diameter and length of the oxidized nanotubes were measured by using SEM, where the sample was prepared by casting a 0.01−0.04 vol % dispersion on a polished SEM stub and drying at room temperature. The dimensions quoted for each sample were the average of measurements on over100 individual nanotubes.

Samples for optical microscopy were prepared by placing a drop of the nanotube dispersion into a cavity in a glass slide, and covering it immediately with a thin glass coverslip to form a sandwich cell which was subsequently sealed using wax or epoxy adhesive. For transmission microscopy, the cells were made very thin to enable sufficient light transmission through the very black samples. Optical microscopy was carried out using a polarized light reflection/transmission microscope (Olympus BX-50). The optical anisotropy was imaged in reflection as "bireflection" , and in transmission as birefringence.

Table 1. Number/Weight Average Values of the Diameter, Length, and Aspect Ratio and Polydispersity of Dispersions A and B

samples		dispersion A	dispersion B
diameter, d, nm	no. average	31	67
	weight average	35	102
	polydispersity	1.14	1.53
length, L, nm	no. average	739	1860
	weight average	976	3065
	polydispersity	1.32	1.65
aspect ratio	no. average	30	40
	weight average	36	67
	polydispersity	1.19	1.67

Results and Discussion

Polydispersity of the Acid Treated MWNTs. The acid treatment introduces oxygen-containing functional groups onto the surface to give a negatively charged surface, particularly through the ionization of the acidic surface groups. The resulting electrostatic repulsive forces enhance the dispersibility and stability of the colloidal suspension in water. The nanotubes after acid treatment are shortened and thinned simultaneously into a certain range, dependent on the temperature of the water bath and the time of ultrasonication, as shown in the histograms of Figure 1. This change is the result of a degree of exfoliation of the outer layers. The data of Figure 1 are summarized in Table 1. The nanotubes in dispersion A, which received the longer treatment (24 h as compared with 12 h for sample B) are shorter,

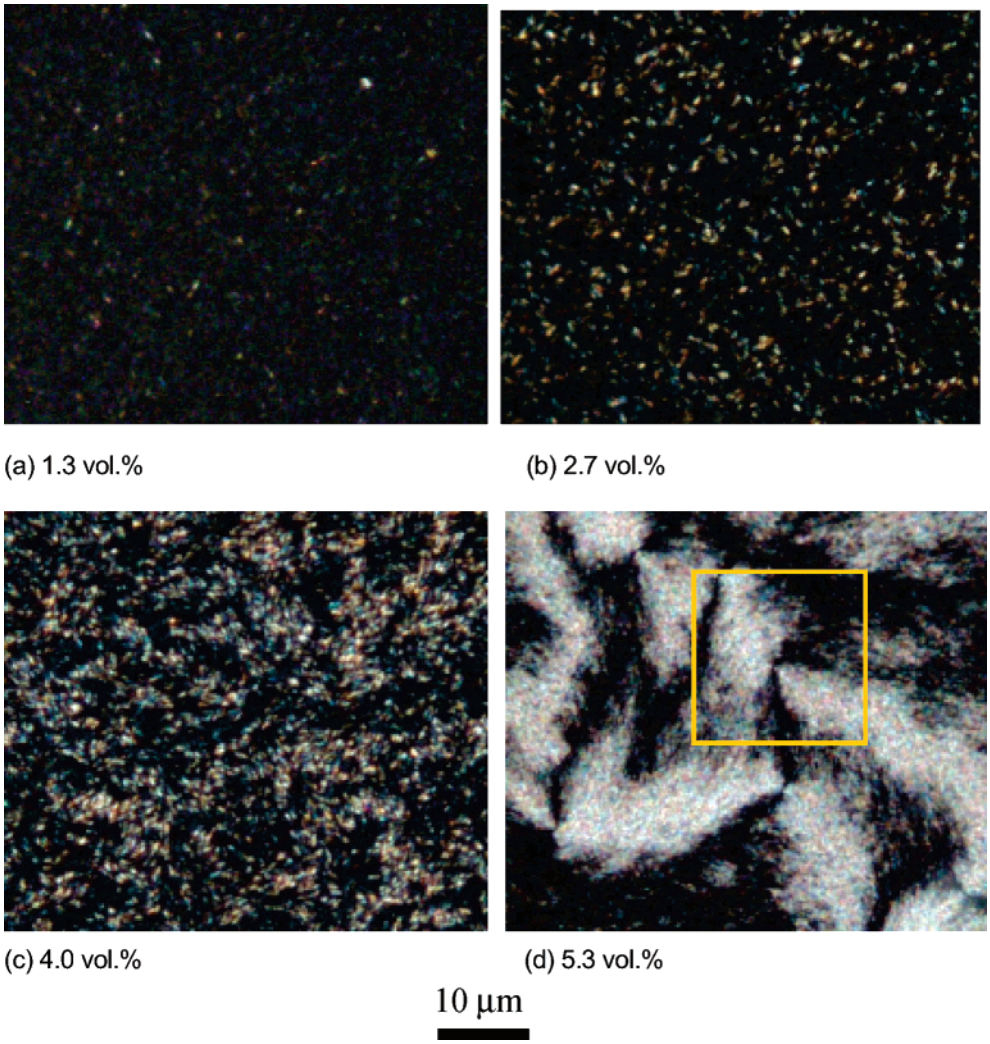

Figure 2. Micrographs of MWNT dispersions A at different aqueous concentrations respectively, imaged in reflected light with crossed polars: (a) 1.3 vol % dispersion, showing weak bireflection contrast from nematic nuclei; (b) 2.7 vol % dispersion, where the discrete entities appear larger and appear to represent growing nematic nuclei; (c) 4.0 vol % dispersion, where the nematic nuclei are beginning to "join up" in some regions; (d) 5.3 vol % dispersion, showing the Schlieren texture of nematic liquid crystals.

thinner and more uniform. than those in the dispersion B.

Isotropic—Nematic Phase Transition as a Function of Concentration. The two samples with different dimensional distribution characteristics gave rise to recognizably different phase transition behavior from isotropic to nematic via an extensive biphasic region.

Sample A. Figure 2 shows suspensions of carbon nanotube dispersion A in reflected light with crossed polars. As concentrations below about 1 vol %, there was very little bireflecting contrast, indicating the isotropic phase. As the concentration was increased above 1 vol %, weak bireflection contrast started to become apparent as discrete bright spots, as shown in Figure 2a. It would appear that some nanotubes were beginning to aggregate to forming local ordered nuclei or "swarms".[30] It should be noted that the visibility in this case (they are not generally seen optically in small-molecule liquid crystalline systems) may be associated with the larger size of the multiwall nanotube entities compared with individual molecules and also, their slower and thus eye-resolvable Brownian motion. As the concentration of the dispersion was increased, the size and volume fraction of the discrete bireflecting regions increased, as shown in Figure 2b, which is a 2.7 vol % sample. At a higher concentration of 4.0 vol %, (Figure 2c) the nematic swarms are beginning to join up into regions of similar optical anisotropy, and thus orientation, although these regions do not propagate continuously through the sample. We suggest that at 4% the anisotropic phase is on the point of becoming continuous, even though there are regions in which the orientation of the swarms is not at all correlated, i.e., regions which are still isotropic. Interestingly, the orientational percolation of isolated anisotropic regions into a continuous anisotropic nematic phase is reminiscent of the predictions of the Lebwohl−Lasher model,[31] where "orientational percolation" of nematic nuclei appears to be the critical point of the phase transition.[32] Figure 2d shows the structure at 5.3% where all the phase is anisotropic, with the different regions changing contrast between bright and dark on rotation of the crossed polars. This structure is a typical Schlieren texture characteristic of nematic liquid crystalline phases. The texture contains a number of distinctive brushlike regions of contrast which emanate from singularities known as disclinations. The brushes seen here rotate at twice the angular velocity of the crossed polars, indicating that the disclinations at their centers are of strength $\pm 1/2$.[33] Some of the brushes rotated in the same sense as the polars, others in the opposite sense, indicating singularities of strength $+1/2$ and strength $-1/2$, respectively. Figure 3 shows

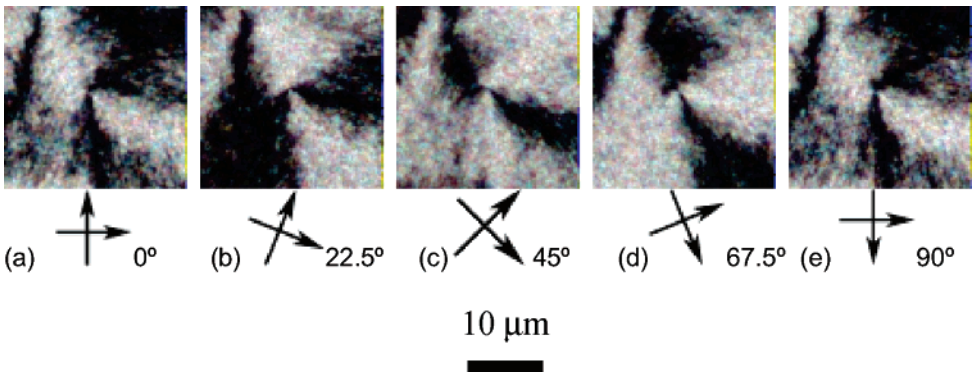

Figure 3. Series of optical micrographs show the effect of a clockwise rotation of the crossed polars on the contrast surrounding a $+1/2$ strength disclination. The region is that delineated by a superimposed box in Figure 2d. Note how the two-bladed "brush" rotates at twice the angular velocity and in the same sense as the crossed polars.

brushes rotating with the crossed polars for a single $+1/2$ disclination.

On the basis of the polarized light microscopy we estimate a biphasic range between 1% and 4% for sample A. While Onsager[34] and Flory[35] have predicted a biphase for monodisperse lyotropic liquid crystals, the region is narrow compared with our observation here, covering typically a 1% concentration range (the so-called "Flory chimney"). The comparatively large range of the biphasic region is presumably associated with polydispersivity in terms of length, diameter, and straightness of the nanotubes, and the possibility of segregation of the more nematogenic tubes to the growing liquid crystalline phase.[35] This fractionation effect has also been observed for polydisperse solutions of TMV,[36] polybenzamides,[37] and poly(phenyleneterephthalamines).[38]

Sample B. This sample had a shorter acid treatment than Sample A, showing a wider distribution of nanotube lengths and a greater average length. An equivalent set of optical bireflection micrographs to Figure 2 are shown for Sample B in Figure 4. In this case, the biphasic region requires a somewhat larger field of view to give a proper representation of the structure and thus the micrographs in Figure 4 are presented at a somewhat lower magnification than those in Figure 2. In the case of specimen B, the biphasic region is yet wider. Parts a−c of Figure 4 show that as the concentration is increased, the nematic-rich nuclei grow and coagulate into large nematic domains which coexist with isotropic regions which remain dark irrespective of the rotation setting of the crossed polars. By 6.5% the structure is largely nematic, the darker and lighter regions of Figure 4d changing contrast on rotation of the crossed polars., as with the Schlieren texture. We suggest that the enhanced segregation effects seen in sample B as compared with A and the larger compositional range of the biphasic region are directly the consequence of the greater polydispersivity of sample B (cf. Figure 1 and Table 1)

Scintillation. The bireflection of nematic domains were always accompanied by visible scintillation under crossed polarized light, which was different from that of small mass liquid crystals and liquid crystalline polymers. The scintillating effect became more obvious in dispersion B with its wider range of nanotube dimensions, particularly at the lower end of the concentration range where the nematic nuclei were isolated in the continuous isotropic phase (Figure 4a). In fact, rapid, incessant and irregular Brownian motion of massive individual nanotubes in the isotropic regions could be directly observed under the normal light microscope under normal illumination. At the same time, the translational motion of the swarms was not marked. The visible Brownian movement in the aqueous dispersion may imply that nanotubes behave particle-like characteristic features. The length of oxidized MWNTs in the dispersion A and B (0.5−2 μm in Figure 1 and Table 1) are much shorter than the estimated persistence length of single wall carbon nanotubes (some tens of micrometers[21,39]), let alone that of MWNTs, and therefore those tubes are logically assumed to approximate to rigid rods. These straight tubes can be considered as analogous to tobacco mosaic virus (TMV) which consists of "Brownian particles" of length 300 nm and diameter 18 nm.[24] Table 2 lists the estimation of rotary diffusivity, the rotational relaxation times of MWNT dispersions in the dilute and semidilute regime on the basis of theoretical analysis of rigid-rod particles[40−42] (see Appendix). Obviously, the rotational relaxation times of dispersions A and B in a semidilute regime fall into the range of the human eye's response rate (> 42 ms, a reciprocal of 24 frame per second for eliminating perceptible flicker by eyes). Taking into account the crowding effect of neighboring tubes in the more concentrated regime, the actual rotational relaxation time of the nanotubes of dispersion A and B in the biphase and nematic phase should be longer than that estimated in semidilute regime. The visible scintillating movement led to some smearing of the images shown in Figures 2−4 (exposure time of $\sim$ 20 s), but this was not extensive as the motion was essentially rotational, not translational. From eq 3 (appendix) and Table 2, it is apparent that both the length of the nanotubes and their mutual interaction has significant influence in slowing their random rotary motion. For example, Brownian rotation of longer nanotubes in dispersion B occurs an estimated one and one-half orders of magnitude more slowly than those in dispersion A, although their length is only around twice as much. This prediction is consistent with the observation that scintillation in dispersion B appeared considerably slower and hence was more easily noticeable than in dispersion A.

Thin Films of Sample A. Reflected microscopy is an appropriate technique for determining the optical properties of generally opaque carbon materials.[20] However, it is possible to make observations in transmitted light in sufficiently thin samples, remembering that the fraction of light transmitted scales as $\exp[-At]$, where

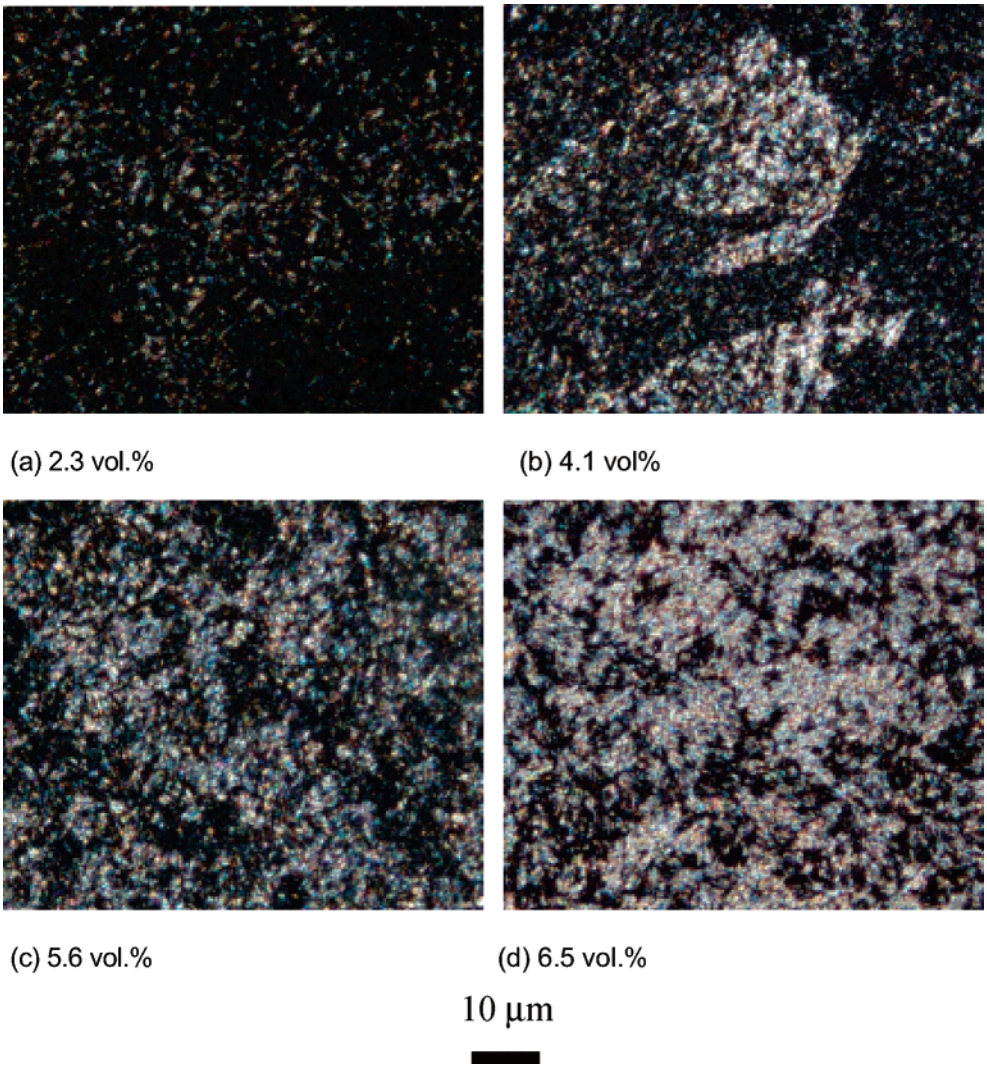

Figure 4. Micrographs of MWNT dispersions B show broadening and phase separation of pre-transitional effects at different aqueous concentrations respectively, imaged in reflected light with crossed polars. (a) 2.3 vol % dispersion, the early stage of nematic nuclei; (b) 4.1 vol % dispersion, the discrete stronger birefringent domains appearing to represent a nematic-rich biphase; (c) 5.6 vol % dispersion, more nematic-rich domains throughout the specimen; (d) 6.5 vol % dispersion, quasi continuous anisotropic texture.

Table 2. Estimation of the Rotary Diffusivity, the Rotational Relaxation Times in the Dilute and Semidilute regime of MWNT Dispersions (See Appendix)

samples		dispersion A	dispersion B	Hyperion[a] MWNT dispersion[27]	TMV[a] aqueous dispersion[23]
dilute regime	rotary diffusivity, D_{r0}, s^{-1}	18.67	1.19	72	233
	rotational relaxation, $\tau_0 \approx 1/(6D_{r0})$, ms	9	140	2	0.7
critical concentration from the dilute to semidilute regime, ν_0, vol %		0.04	0.03	0.002	0.09
semidilute regime	rotational relaxation time, $\tau_s \approx 1/D_{r0}$, ms	54	840	10	4

[a] The oxidized Hyperion MWNTs were 1.1 μm in length and 10 nm in diameter;[27] TMV, 300 nm in length and 18 nm in diameter.[24]

t is the thickness.[44] It was found that despite the high optical absorbency of suspensions of carbon nanotubes, the nematic dispersion could become sufficient transparent for transmission polarizing microscopy at thicknesses below 20−10 μm. Figure 5a is a thin sample of sample A of concentration 5.3 vol %, between crossed polars. The texture in Figure 5a appears different from that observed under reflection light which is more typically Schlieren (e.g., Figure 2d); it is finer and much more similar to that seen from liquid crystalline polymers where it has been known as a tight texture.[45] The presence of two surfaces encasing a very thin sample is thought here to pin the topological structure preventing it relaxing to a typical Schlieren texture. (In the case of liquid crystalline polymers, it may be restrictions on internal kinetic mobility, which provides the constraint.)

Toward the edges of the thin, liquid sample (Figure 5b), the orientation tends much more to a monodomain with line features giving rise to birefringent contrast. For conventional liquid crystals such textures are often induced in electrical or magnetic fields or by shearing flow.[30] In this case, it is possible that the surface tension may be responsible for the higher degree of alignment at the edge of the thin layer of the dispersion, an indication that nanotubes in liquid crystalline dispersions may also be oriented by external fields.

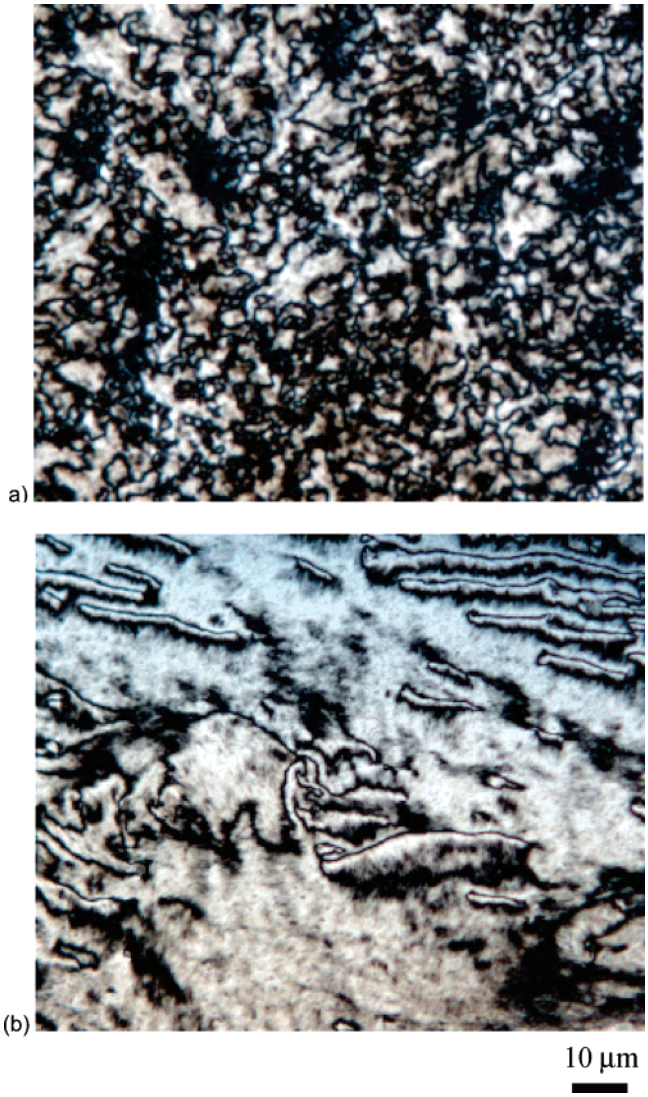

Figure 5. (a) Birefringence texture of a thin layer of the nematic dispersion A (5.3 vol %), imaged in transmitted light with crossed polars. (b) Wall texture at the edge of a thin layer of the nematic dispersion A (5.3 vol %), imaged in transmitted light with crossed polars.

When thin films were dried by evaporation from a single substrate, the basic topological structure was retained. This observation is in accord with liquid crystalline polymers which, when solidified either by solvent removal or cooling in the case of thermotropic materials, the texture typical of the liquid crystal state remains, although there may be localized areas of higher (crystalline type) order.[45−48] Figure 6 (sample A original dispersion of 5.3 vol %) shows that the bireflection Schlieren texture is still retained after the water has been evaporated slowly at the room temperature. However, in addition to the retained texture, the drying process appears in this example to have introduced an additional array of fine periodic stripes, which were apparent with or without crossed polars and did not change their orientation when rotating the crossed polars. These stripes are thought to be the result of drying a thin film adhering to, and thus constrained by a substrate. (The drying process will reduce the volume of the sample by a factor of ~ 20) It is straightforward to analyze the texture on rotation of the polars and recognize the sign and the structure of the disclinations in the nematic phase, such as a $-1/2$ disclination

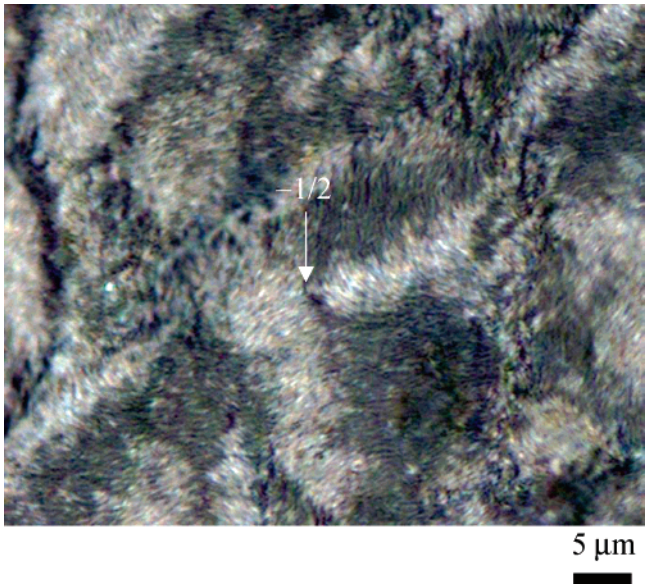

Figure 6. Bireflection texture of the dried nematic CNT film under crossed polarized light. Considerable detail of nanotube orientation is visible through the almost periodical stripes, revealing the structures of disclinations with topological strength −1/2 (a).

example of Figure 6. The optical analysis also confirms that the optical stripes, which became apparent on drying, lie parallel to the long axis of nanotubes.

Scanning Electron Microscopy of Dried Film Specimens. It has already been explained that the texture seen in the liquid crystalline dispersion is retained on drying. However, such specimens additionally provide a unique opportunity for study of the detailed structure by FEGSEM at a resolution sufficient to resolve the individual nanotubes. Such an opportunity is not available for conventional or polymeric liquid crystals, where the essential organizing elements, the molecules, are not only smaller but would be subject to severe beam damage at the high magnification necessary. The detailed structure of a plus/minus disclination pair is clearly seen in Figure 7a. The nanotubes are constrained to lie in the plane of the film so that disclinations have a wedge character and only the bend and the splay distortions are apparent. Furthermore, the stripes parallel to the axes of the nanotubes, appear to be identifiable with fissures left between the nanotubes on drying. Figure 7b is a FEGSEM image of a dried film, but in this case close to the edge of the specimen, from a region similar to that which gave the transmission optical image of Figure 5b before evaporation of the water. The more uniform orientation together with the wavelike disturbances is clearly visible.

Summary

Multiwall carbon nanotubes, when in stable dispersion, show long-range nematic orientational order, and the isotropic/nematic phase change (as a function of concentration) shows many similarities to lyotropic dispersions of rodlike molecules. The width of biphasic region is held to be a consequence of the considerable polydispersity of the nanotube samples used. It is certainly wider in the sample with a greater range of nanotube lengths and diameters. The details of the Schlieren texture in the nematic phase have been examined using both reflected and transmitted light microscopy. The optical anisotropy of the texture indi-

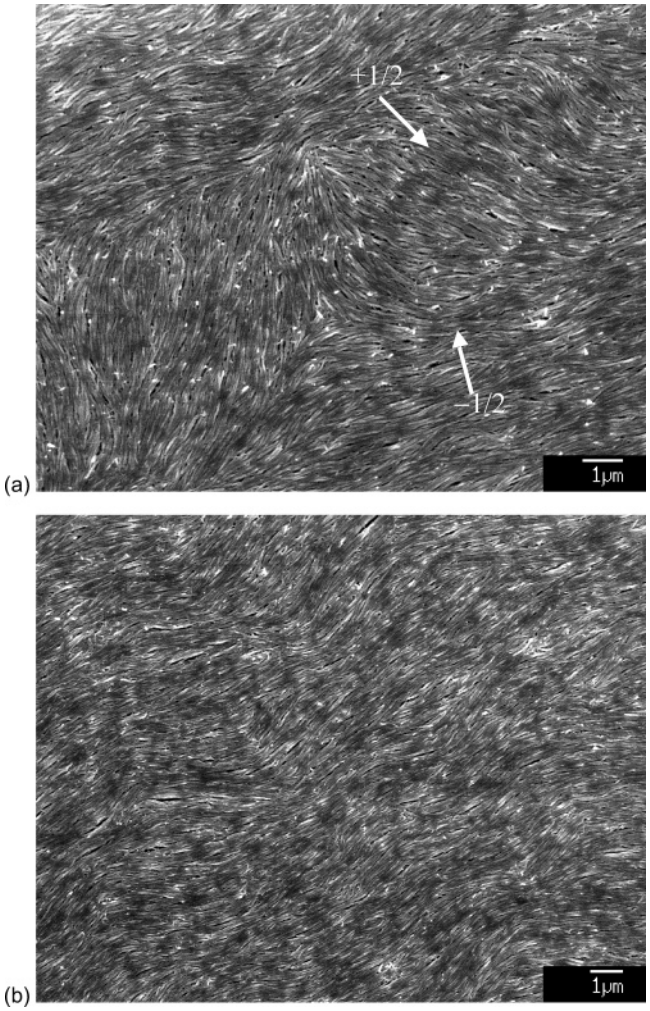

Figure 7. Scanning electron micrographs of a dried nematic MWNT film showing (a) the director fields around a pair of disclinations of topological strength $+1/2$ and $-1/2$ and (b) the region toward the edge of the film which is free of disclinations and corresponds with the observations made in polarized light (Figure 5b).

cates the multidomain alignment with a number of singularities. In carefully dried samples, the topological texture is retained, and the detailed nature of the disclination singularities becomes amenable to high-resolution scanning electron microscopy. The resultant resolution of the individual carbon nanotubes offers a unique opportunity to view the disclination core structure, a study that will feature in a future paper.

Acknowledgment. We thank D. Nicol for his help in scanning electron microscopy, and for Dr. M. Shaffer, Dr. I. Kinlock and K. Koziol for helpful discussions. This work was supported by the Cambridge-MIT Institute.

Appendix

In the dilute region of rodlike particle dispersions, the coefficient ζ is a viscous drag coefficient, which for long, slender fibers is given by Batchelor[42]

$$\zeta = \frac{\pi\eta_s L^3}{6\ln(2L/d)} f(\epsilon) = \frac{k_B T}{2D_{r0}} \tag{1}$$

with $\epsilon \equiv [\ln(2L/d)]^{-1}$, and

$$f(\epsilon) = \frac{1 + 0.64\epsilon}{1 - 1.5\epsilon} + 1.659\epsilon^2 \tag{2}$$

where d is the rod diameter, L is the length of the rod, k_B is Boltzmann's constant, η_s is the solvent viscosity, and T is temperature. Thus, the rotary diffusivity of the rods in the dilute solution works out to be

$$D_{r0} = \frac{3k_B T\ln(2L/d)}{\pi\eta_s L^3 \mathrm{f}(\epsilon)} \tag{3}$$

In the dilute regime, the rotational relaxation time of the rod can be estimated via $\tau_0 \approx 1/(6D_{r0})$. The transition from dilute to semidilute regime should occur when $\nu_1 \approx 24(d/L)^2$, where ν_1 is the volume fraction of the rod particles, d and L are the diameter and length of the nanotube.[40] As the dispersion is made more concentrated and transferred into to the semidilute regime, the rotational time of the rod is impeded, and approximated to $\tau_s \approx 1/D_{r0}$.[40] Table 2 gives the list of the estimated values of the rotational diffusivity and relaxation times in these two regimes. For comparison, estimated values of the rotational diffusivity and relaxation times for Hyperion multiwall nanotubes[27] and the tobacco mosaic virus (TMV) are also listed in Table 2.

References and Notes

(1) Song, W.; Kinloch, I.; Windle, A. H. *Science* **2003**, *302*, 1363−1363.
(2) Harris, P. *Carbon Nanotubes and Related Structures*; Cambridge University Press: Cambridge, U.K., 1999.
(3) Li, W. Z.; Xie, S. S.; Qian, L. X.; Chang, B. H.; Zou, B. S.; Zhou, W. Y.; Zhao, R. A.; Wang, G. *Science* **1996**, *274*, 1701−1703.
(4) Jiang, K.; Q. Li, Q.; Fan, S. *Nature (London)* **2002**, *419*, 801−801.
(5) Li, Y.; Kinloch, I.; Windle, A. H. *Science* **2004**, *304*, 276−278.
(6) Hirsch, A. *Angew. Chem., Int. Ed.* **2002**, *41*, 1853−1859.
(7) Ajayan, P. M.; Stephan, O.; Colliex, C.; Trauth, D. *Science* **1994**, *265*, 1212−1214.
(8) Vigolo, B.; Penicaud, A.; Coulon, C.; Sauder, C.; Pailler, R.; Journet, C.; Bernier, P.; poulin, P. *Science* **2000**, *290*, 1331−1334.
(9) Kumar, S.; Dang, T. D.; Arnold, F. E.; Bhattacharyya, A. R.; Min, B. G.; Zhang, X.; Vaia, R. A.; Park, C.; Adams, W. W.; Hauge, R. H.; Smalley, R. E.; Ramesh, S.; Willis, P. A.; et al. *Macromolecules* **2002**, *35*, 9039−9043.
(10) Dalton, A. B.; Collins, S.; Munoz, E.; Razal, J. M.; Ebron, V. H.; Ferraris, J. P.; Coleman, J. N.; Kim, B. G.; Baughman, R. H. *Nature (London)* **2003**, *423*, 703−703.
(11) de Heer, W. A.; Bacsa, W.; Gerfin, T.; Baker, R. H.; Forro, L.; Ugarte, D. *Science* **1995**, *268*, 845−847.
(12) Li, Y.-H.; Xu, C.; Wei, B.; Zhang, X.; Zheng, M.; Wu, D.; Ajayan, P. M.; *Chem. Mater.* **2002**, *14*, 483−485.
(13) Shimoda, H.; Oh, S. J.; Geng, H. Z.; Walker, R. J.; Zhang, X. B.; McNeil, L. E.; Zhou, O. *Adv. Mater.* **2002**, *14*, 899−901.
(14) Nagahara, L.; Amlani, I.; Lewenstein, J.; Tsui, R. K. *Appl. Phys. Lett.* **2002**, *80*, 3826−3828.
(15) Walters, D. A.; Casavant, M. J.; Qin, X. C.; Huffman, C. B.; Boul, P. J.; Ericson, L. M.; Haroz, E. H.; O'Connell, M. J.; Smith, K.; Colbert, D. T.; Smalley, R. E. *Chem. Phys. Lett.* **2001**, *338*, 14−20.
(16) Wang, B.; Shankar, R.; Wang, Z.; Liang, Z.; Zhang, C.; Kramer, L. *Mater. Res. Soc. Symp. Proc.* **2004**, *788*, Q10.1.1-Q10.1.9.
(17) O'Connell, M. J.; Peter Boul, P.; Ericson, L. M.; Huffman, C.; Wang, Y.; Erik Haroz, E.; Kuper, C.; Tour, J.; Ausman, K. D.; Smalley, R. E. *Chem. Phys. Lett.* **2001**, *342*, 265−271.
(18) Lynch, M. D.; Patrick, D. *Nano Lett.* **2002**, *2*, 1197−1201.
(19) Lui, T.; Kumar, S. *Nano Lett.* **2003**, *3*, 647.
(20) Hurt, R. H.; Chen, Z. *Phys. Today* **2000**, *March*, 39−44.
(21) Davis, V. A.; Ericson, L. M.; Parra-Vasquez, A. N. G.; Fan, H.; Wang, Y.; Prieto, V.; Longoria, J. A.; Ramesh, S.; Saini,

R. K.; Kittrell, C.; Billups, W. E.; Adams, W. W.; Hauge, R. H.; Smalley, R. E.; Pasquali, M. *Macromolecules* **2004**, *37*, 154−160.
(22) Singh, C.; Shaffer, M. S. P.; Windle, A. H. *Carbon* **2003,** *41* 359−368.
(23) Brian, A. A.; H. L. Frisch, H. L.; L. S. Lerman, L. S. *Biopolymers* **1981**, *20*, 1305−1328.
(24) Bawden, F. C.; Pirie, N. W.; Bernal, J. D.; Frankuchen, I. *Nature (London)* **1936**, Dec., 1051−1052.
(25) Zasadzinski, J. A. N.; Sammom, M. J.; Meyer, R. B.; Cahoon, M.; Caspar, D. L. D. *Mol. Cryt. Liq. Cryst.* **1986**, *138*, 211−229.
(26) Shaffer, M. S. P.; Fan, X.; Windle, A. H. *Carbon* **1998**, *36*, 1603−1612.
(27) Shaffer, M. S. P.; Windle, A. H. *Macromolecules* **1999**, *32*, 6864−6866.
(28) Liu, J.; Rinzler, A. G.; Dai, H.; Hafner, J. H.; Bradley, R. K.; Boul, P. J.; Lu, A.; Iverson, T.; Shelimov, K.; Huffman, C. B.; Rodriguez-Macias, F.; Shon, Y.; Lee, T. R.; Colbert, D. T.; Smalley, R. E. *Science* **1998**, *280*, 1253−1256.
(29) Shaffer, M. S. P.; Koziol, K. *Chem. Commun.* **2002**, *18*, 2074−2075.
(30) de Gennes, P. G. *The Physics of Liquid Crystals*, Clarendon: Oxford, U.K., 1993.
(31) Lebwohl, P. A.; Lasher, G. *Phys. Rev. A* **1972**, *6*, 426−429.
(32) Gonin, D.; Windle, A. H. *Liq. Cryst.* **1997**, *23*, 489−502.
(33) Frank, F. C. *Discuss. Faraday. Soc.* **1958**, *25*, 1−28.
(34) Onsager, L. *Ann. N.Y. Acad. Sci.* **1949**, *56*, 627−659.
(35) Fory, P. J. *Proc. R. Soc. A* **1956**, *243*, 73−89.
(36) Oster, G. *J. Gen. Physiol* **1950**, *33*, 445−452.
(37) Kwolek, S. L.; Morgan, P. W.; Schaefgen, J. R.; Gulrich, L. W. *Macromolecules* **1977**, *10*, 1390−1396.
(38) Bair, T.; Morgan, P. W.; Killian, J. L. *Macromolecules* **1977**, *10*, 1396−1400.
(39) Hamm, M.; J. A. Elliott, J. A.; Windle, A. H. *Mater. Res. Soc. Symp. Proc.* **2004**, *788*, L10.11.1−L10.11.6.
(40) Larson, R. G. *The Structure and Rheology of Complex Fluids*; Oxford University Press: Oxford, U.K.,1999.
(41) Doi, M.; Edwards, S. F. *The Theory of Polymer Dynamics*; Oxford Press: New York, 1986.
(42) Batchelor, G. K. *J. Fluid Mech.* **1970**, *41*, 545−557.
(43) Sonin, A. S. *J. Mater. Chem.* **1998**, *8*, 2557−2574.
(44) Hallimond, A. F. *The Polarizing Microscope*; Vickers Ltd.: York, 1970.
(45) Donald, A. M.; Windle, A. H. *Liquid Crystalline Polymers*; Cambridge University Press: Cambridge, U.K., 1992.
(46) Wood, B. A.; Thomas, E. L. *Nature (London)* **1984**, *324*, 655−656.
(47) Chen, S.; Song, W.; Jin, Y.; Qian, Y. *Liq. Cryst.* **1993**, *15*, 247−254.
(48) Song, W.; Fan, X.; Windle, A. H.; Chen, S.; Qian, R. *Liq. Cryst.* **2003**, *30*, 765−774.

MA047691U